journal

J. Am. Ceram. Soc., **81** [8] 2061–70 (1998)

Effect of Starting Powder on Damage Resistance of Silicon Nitrides

Seung Kun Lee,*,† Kee Sung Lee,‡ and Brian R. Lawn*

Materials Science and Engineering Laboratory, National Institute of Standards and Technology, Gaithersburg, Maryland 20899

Do Kyung Kim*

Department of Materials Science and Engineering, Korea Advanced Institute of Science and Technology, Yusong, Taejon 305-701, Korea

The role of starting powder in the resistance of silicon nitride (Si_3N_4) ceramics to strength-impairing contact damage is studied. Si_2N_4 materials are prepared from three starting powders, at selectively increasing hot-pressing temperatures to coarsen the microstructures: (i) from relatively coarse α-phase powder, essentially equiaxed α-Si_3N_4 grains, with limited, slow transformation to β-Si_3N_4 grains toward the latter half of the temperature range; (ii) from relatively fine α-phase powder, a more rapid transformation to β-Si_3N_4, with attendant grain elongation; (iii) from fine β-phase powder, an essentially equiaxed β-Si_3N_4 structure over the entire temperature range. The resulting microstructures thereby provide a spectrum of β/α phase ratios and grain sizes and shapes for investigation. Indentations with hard spheres (Hertzian test) are used to induce damage into the Si_3N_4 specimens. Examination of the indentation sites indicates a competition between brittle and quasi-plastic damage modes: in structures with relatively equiaxed grains, the damage takes the form of classical cone cracking; in structures with large elongate grains, the damage is distributed beneath the contact as grain-localized microfailures within a subsurface ''yield'' zone. Bend tests on specimens containing single-cycle contact damage reveal those structures with well-developed cone cracks to be highly susceptible to strength degradation. The microstructures with the greatest resistance to strength loss are those formed from fine α-phase starting powder at intermediate firing temperatures (1700°C), with characteristic large, elongate β grains. Implications of the results in the context of other mechanical properties, e.g., toughness, wear, and fatigue resistance, are discussed.

I. Introduction

SILICON NITRIDE (Si_3N_4) has been studied extensively for two decades because of its attractive combination of mechanical properties, such as strength, toughness, and wear and fatigue resistance. It is recognized that microstructure is central to these mechanical properties.[1–13] Nevertheless, the role of microstructure remains poorly understood in Si_3N_4 ceramics, because of the complex interplay between such variables as grain size and aspect ratio, ratio of α to β phase, and composition of glassy second phase—generally, these microstructural variables tend to vary in an interdependent manner during the sintering process. When α-Si_3N_4 is used as a starting powder, transformations to β-Si_3N_4 during sintering result in pronounced grain elongation.[2,14,15] In turn, elongated grain structures give rise to enhanced long-crack toughness (strong *R*-curve).[5,7,10,11,13,16] However, this improvement in toughness does not usually extrapolate back to the domain of short cracks, where important properties like strength[17–20] and wear[21] are determined. In this light, there is a need for exploring routes to the microstructural design of Si_3N_4 for improved damage resistance properties at the microscale.

This paper investigates the specific roles of β/α phase ratio and grain size and shape on damage accumulation in Si_3N_4. We achieve control of these microstructural variables via the Si_3N_4 starting powders[11] (but keeping the composition of oxide sintering additives fixed) and by varying the sintering temperature. By choosing powders of different initial phase content and particle size, the following microstructures are produced with increasing temperature: from relatively coarse α-Si_3N_4 starting powder, a progressively coarsening, equiaxed α-Si_3N_4 structure, but with limited, slow transformation to β-Si_3N_4 toward the latter half of the temperature range; from relatively fine α-Si_3N_4 starting powder, a much more rapid transformation to β-Si_3N_4, with attendant grain elongation and coarsening; from fine β-Si_3N_4 starting powder, an essentially equiaxed β-Si_3N_4 structure over the entire temperature range, with progressive coarsening. Selected hot-pressing temperatures between 1570° and 1800°C provide a matrix of microstructures covering a spectrum of β/α ratios and grain geometries for systematic analysis.

To characterize damage accumulation of the Si_3N_4 microstructures we use indentations with spheres (Hertzian test). The Hertzian test has shown itself to be a powerful means of identifying and quantifying damage in ceramics,[22–26] including Si_3N_4.[20,27,28] It reveals in a most compelling manner the critical role of microstructure on the competition between classical cracking (ring, or cone fracture) and quasi-plastic damage (distributed shear-activated microfaulting).[29] Distinction between these two damage modes is directly relevant to applications where highly concentrated loads occur, e.g., in bearings. Indications are that the damage mode in Si_3N_4 progresses from cracking to quasi-plasticity as the microstructure coarsens and elongates,[20,27] and as the β/α ratio increases.[27] By examining these trends in the present structures we illustrate how crucial control of starting powders can be in the design of Si_3N_4 ceramics for damage resistance.

R. K. Bordia—contributing editor

Manuscript No. 190858. Received July 8, 1997; approved November 19, 1997.
Supported by the U.S. Air Force Office of Scientific Research and by the Korea Science and Engineering Foundation.

*Member, American Ceramic Society.
†Guest Scientist from the Department of Materials Science and Engineering, Lehigh University, Bethlehem, Pennsylvania 18015. Now at Advanced Materials Technology, Technical Center, Caterpillar Inc., Mossville, Illinois 61552.
‡Graduate student in the Department of Materials Science and Engineering, Korea Advanced Institute of Science and Technology, Yusong, Taejon 305-701, Korea.

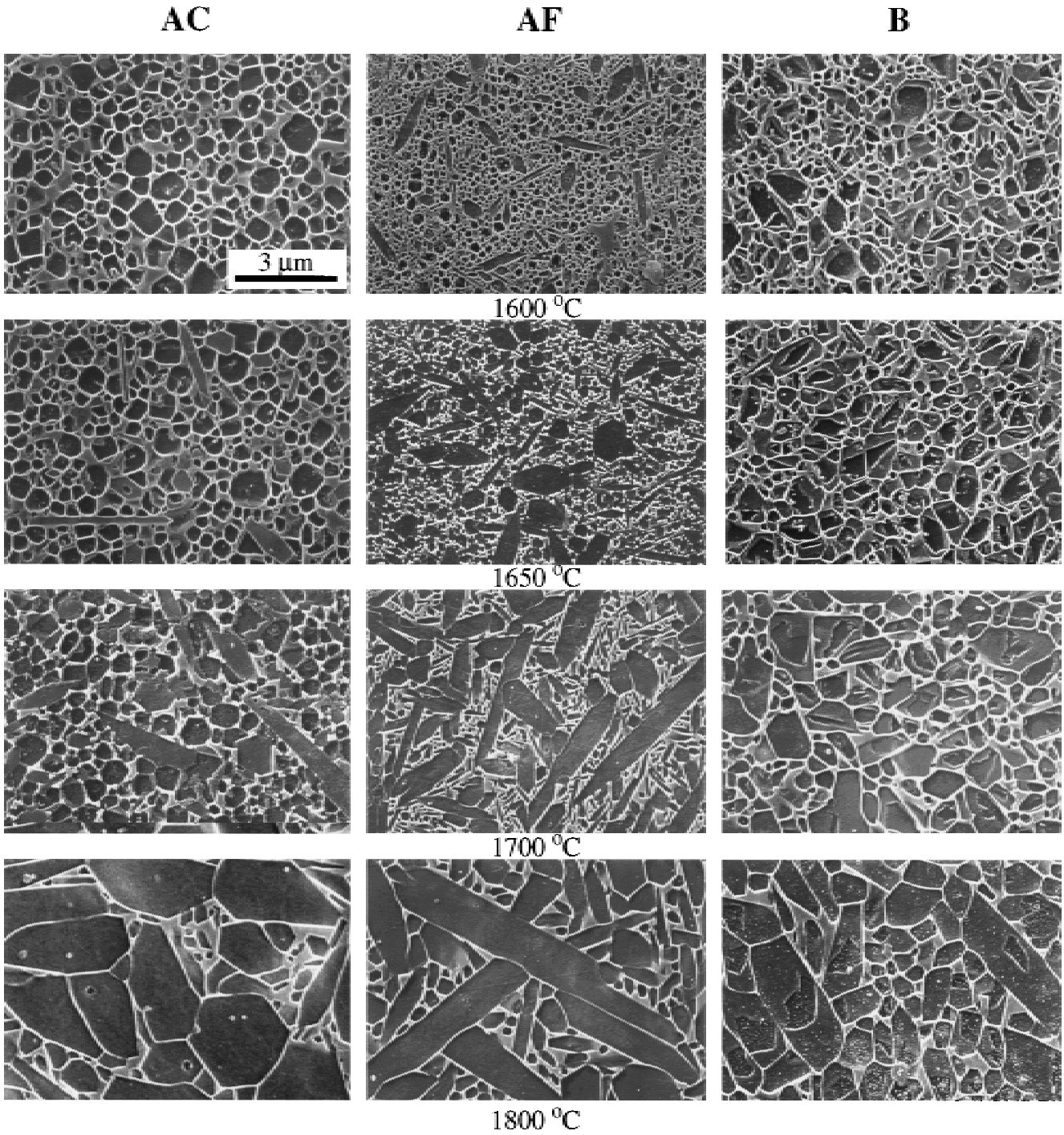

Fig. 1. SEM micrographs of Si_3N_4 polished surfaces, fired at 1600°, 1650°, 1700°, and 1800°C for 1 h. Specimen designation as follows: **AC** (E3 powder, α phase, coarse); **AF** (E10 powder, α phase, fine); **B** (KSN-80SP powder, β phase). Specimens plasma etched in CF_4 and O_2 gas for 10 min to reveal grain structures.

II. Experimental Procedure

(1) Materials Processing and Preparation

Three starting silicon nitride powders were used: relatively coarse α-Si_3N_4 (UBE-SN-E3, mean particle size 1.0 μm, Ube Industries, Tokyo, Japan), with ≈5 vol% β-Si_3N_4; relatively fine α-Si_3N_4 (UBE-SN-E10, mean particle size 0.3 μm, Ube Industries, Tokyo, Japan), again with ≈5 vol% β-Si_3N_4; and β-Si_3N_4 (KSN-80SP, mean particle size 0.5 μm, ShinEtsu, Tokyo, Japan), with ≈20 vol% α-Si_3N_4. Sintering additives, 5 wt% Y_2O_3 (Fine Grade, H. C. Starck GmbH, Goslar, Germany), 2 wt% Al_2O_3 (AKP50, Sumitomo Chemical Co. Ltd., Tokyo, Japan), and 1 wt% MgO (High Purity, Baikowski Co., NC), were mixed with each starting powder. The mixed batches were ground as slurries in 2-propanol for 24 h in a planetary mill using zirconia balls in a polypropylene container. After drying, the softly agglomerated powders were crushed and sieved through a 60-mesh screen. These resulting mixes were designated according to the Si_3N_4 starting powders: **AC** (E3 powder, α phase, coarse); **AF** (E10 powder, α phase, fine); **B** (KSN-80SP powder, β phase).

Hot pressing of sample blocks with 50 mm diameter and 5 mm thickness from each powder batch was performed in nitrogen gas at 1 atm under uniaxial compression 30 MPa in

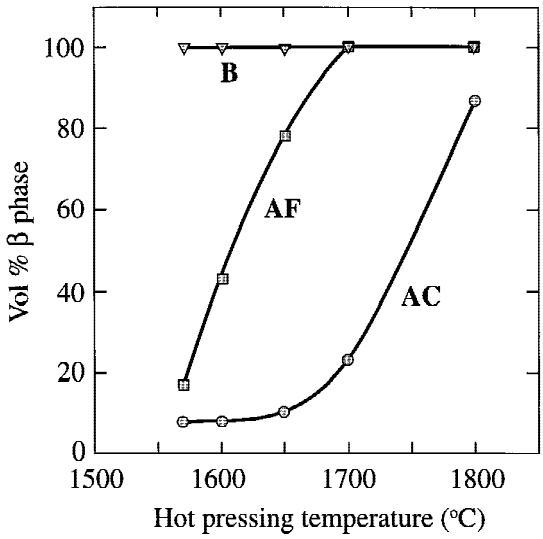

Fig. 2. XRD determination of volume fractions of β and α phases in **AC**, **AF**, and **B** Si_3N_4 (see Fig. 1), as function of hot-pressing temperature.

a graphite die, at 1570°, 1600°, 1650°, 1700°, and 1800°C for 1 h. Top and bottom surfaces of the fired blocks were ground on a diamond wheel, and the blocks diamond sawn into bars 25 mm × 4 mm × 3 mm for evaluation and testing.

Specimen surfaces were polished normal to the hot-press direction to 1 μm finish for characterization. These surfaces were plasma etched to highlight the grain structures. After gold coating, the etched surfaces were examined by scanning electron microscopy (SEM), and grain sizes and shapes determined from micrographs using an image analyzer (Bioscan OPTIMAS 4.1, Bioscan Inc., Edmonds, WA), as follows: mean grain sizes, from linear intercepts over all grain boundaries; aspect ratios, as length/width of the 10% largest elongate β grains;[14] volume fractions, from grain area determinations of all β grains with aspect ratio ≥3.[12] X-ray diffraction (XRD) was used to determine the β/α phase ratio for each material.

Densities were measured using the Archimedes method.

(2) Mechanical Testing

Hertzian contact tests were made on polished Si_3N_4 surfaces to determine damage characteristics.[27] In these tests, tungsten carbide (WC) spheres of radius $r = 1.98$ mm were used at peak loads up to $P = 4000$ N and at fixed crosshead speed 1.67 $\mu m \cdot s^{-1}$. The WC spheres themselves tended to deform during indentation,[30] so were constantly rotated and ultimately replaced. Section views of the damage patterns were obtained using bonded-interface specimens.[23,24] These specimens were prepared by bonding together two polished half-bars at a common interface with a thin layer of adhesive, and then polishing the top surfaces. Rows of indentations were then made on these top surfaces, symmetrically along the surface trace of the bonded interface. The adhesive was dissolved in acetone, and the top and side surfaces of the separated half-blocks gold coated for optical examination in Nomarski illumination. Supplementary observations of the damage were made using SEM to determine the basic nature of the cracking and quasi-plasticity in relation to the microstructure.[20]

Additional indentation tests were made with the same WC spheres on polished surfaces of each of the Si_3N_4 materials, to obtain critical loads for ''yield,'' P_Y, and for cracking, P_C. The critical configurations were determined by examining the postindented surfaces over a range of loads, and searching for the signs of first damage.[27] Nomarski examination of surfaces

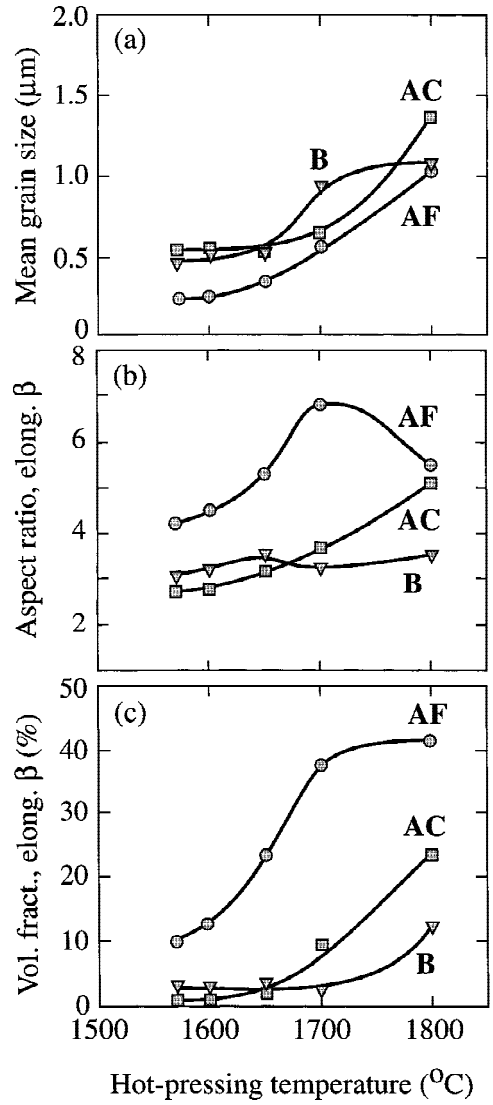

Fig. 3. Microstructural characterization of **AC**, **AF**, and **B** Si_3N_4 materials as function of hot-pressing temperature: (a) mean grain size, (b) aspect ratio of largest 10% elongate β grains, (c) volume fraction of elongate β grains with aspect ratio >3.

gold-coated after indentation was again used for this purpose. Acoustic detectors were also useful for detecting the critical pop-in load for full cone cracks.[27]

Strength tests were made on sets of Si_3N_4 specimens fired at 1700°C, to quantify the degrading effects of the contact damage.[28] Four-point bend tests were made on polished and prechamfered bars (25 mm × 4 mm × 3 mm, inner span 10 mm and outer span 20 mm), with the indented surfaces on the tensile side. The contact damage itself was made over a load range $P = 0$–4000 N. Specimens were covered by a drop of silicon oil before testing, and were broken in fast fracture (<10 ms), to avoid the influence of moisture (''inert'' strengths). Broken specimens were examined fractographically in Nomarski illumination to locate the source of failure, i.e., indentations or other sites.

Routine measurements of Young's modulus (sonic method) and hardness (load/projected area, Vickers indenter[31]) were carried out on these specimens.

III. Results

(1) Materials Characterization

Results of the microstructural characterization are shown in Figs. 1–3. Figure 1 shows scanning electron microscopy (SEM)

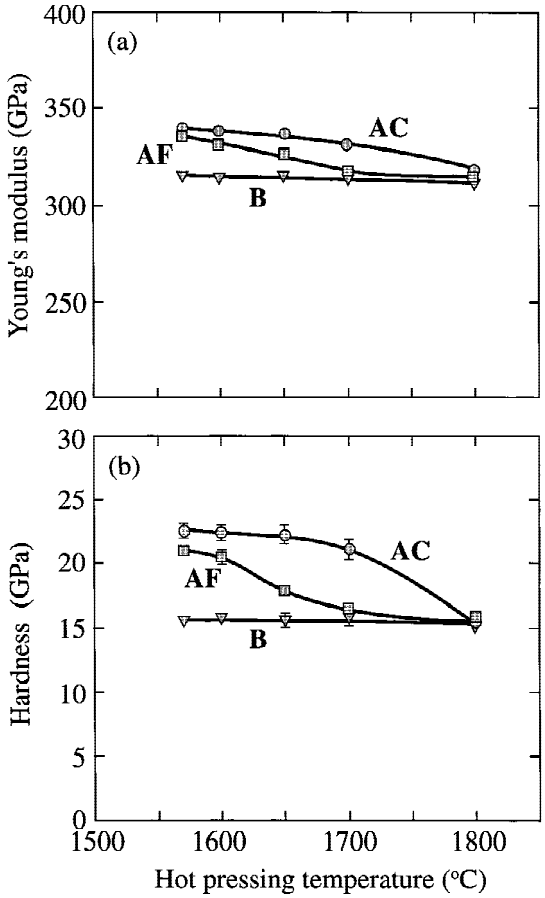

Fig. 4. Plot of (a) Young's modulus and (b) hardness of **AC**, **AF**, and **B** Si_3N_4 materials as function of hot-pressing temperature.

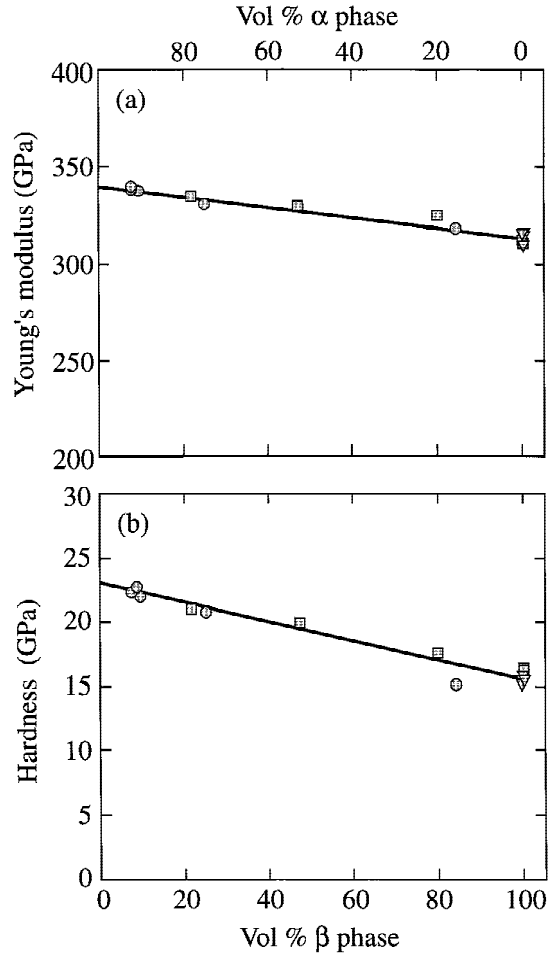

Fig. 5. Replot of (a) Young's modulus and (b) hardness data from Fig. 4 as function of volume fractions of β and α phases.

micrographs of the different Si_3N_4 microstructures for each starting powder:

(i) **AC** Si_3N_4. After hot pressing at 1600°C, this material reveals a microstructure with mainly equiaxed α grains of mean grain size ≈0.6 μm, but with minor β phase. At 1650°C, the equiaxed α grains are larger, but occasional elongate β grains are now apparent. At 1700°C, the β grains continue their elongated growth, but the α phase still dominates. Finally, at 1800°C, the β phase dominates, but the structure is again predominantly equiaxed.

(ii) **AF** Si_3N_4. At 1600°C, the material contains mainly equiaxed α grains of mean grain size ≈0.2 μm, but some elongated β grains are already apparent. At 1650°C these β grains have continued their elongate growth, but at a much faster rate than in **AC** Si_3N_4; the smaller α grains have also begun to transform to β phase. At 1700°C, the β phase is dominant. At 1800°C, the β grains enlarge further, as in **AC**, but remain elongate.

(iii) **B** Si_3N_4. At 1600°C, the structure consists totally of equiaxed β grains, mean grain size ≈0.5 μm. On heating through 1800°C, the β phase persists, and the microstructures enlarge but remain predominantly equiaxed with just occasional elongate grains.

Density determinations indicate a porosity level <0.1% in all microstructures in Fig. 1.

Figure 2 plots volume percent β and α phase for the three Si_3N_4 starting powder types as a function of hot-pressing temperature, from XRD. In **AC** Si_3N_4 an α → β transformation takes place, but is relatively sluggish, accelerating only above 1700°C (note that some α phase remains even at 1800°C). The same transformation occurs in **AF** Si_3N_4, but much more rapidly, reaching completion at 1700°C. There is no detectable phase transformation at all in **B** Si_3N_4; the β phase dominates over the entire temperature range.

Mean grain sizes and aspect ratios are plotted for the Si_3N_4 materials as a function of hot-pressing temperature in Fig. 3. Overall mean grain sizes (Fig. 3(a)) increase steadily with temperature in all three materials. Aspect ratios (Fig. 3(b)) and volume fractions (Fig. 3(c)) of the elongate β grains increase strongly with temperature in the **AF** material to 1700°C, and increase only slightly, above 1700°C, in the **B** material, with **AC** intermediate. Note especially the dominant population of elongate β grains in **AF** at 1700°C.

Figure 4 plots Young's modulus and hardness against hot-pressing temperature for each material. Both modulus (Fig. 4(a)) and hardness (Fig. 4(b)) decline with temperature: in **AC** Si_3N_4, starting with relatively high values at 1570°C, declining only slightly between 1570° and 1700°C, and finally falling off between 1700° and 1800°C; in **AF** Si_3N_4, starting a little lower at 1570°C, but declining much more quickly, and approaching a similar reduced level at 1700°C; in **B** Si_3N_4, starting low and staying low over the temperature range. Noting the (inverse) correlation of the curves in Fig. 4 with those in Fig. 2, we replot the modulus and hardness data as a function of phase content in Fig. 5. The results are consistent with a ''rule of mixtures'': for modulus (Fig. 5(a)), between extrapolation limits of high-modulus α phase (340 GPa) and low-modulus β phase (312 GPa);[32] for hardness (Fig. 5(b)), between extrapolation limits of high-hardness α phase (23.1 GPa) and low-hardness β phase (15.5 GPa).[33] Note that whereas the trends are similar in Figs. 4 and 5, the rate of decline relative to temperature is considerably faster in the hardness than in the modulus.

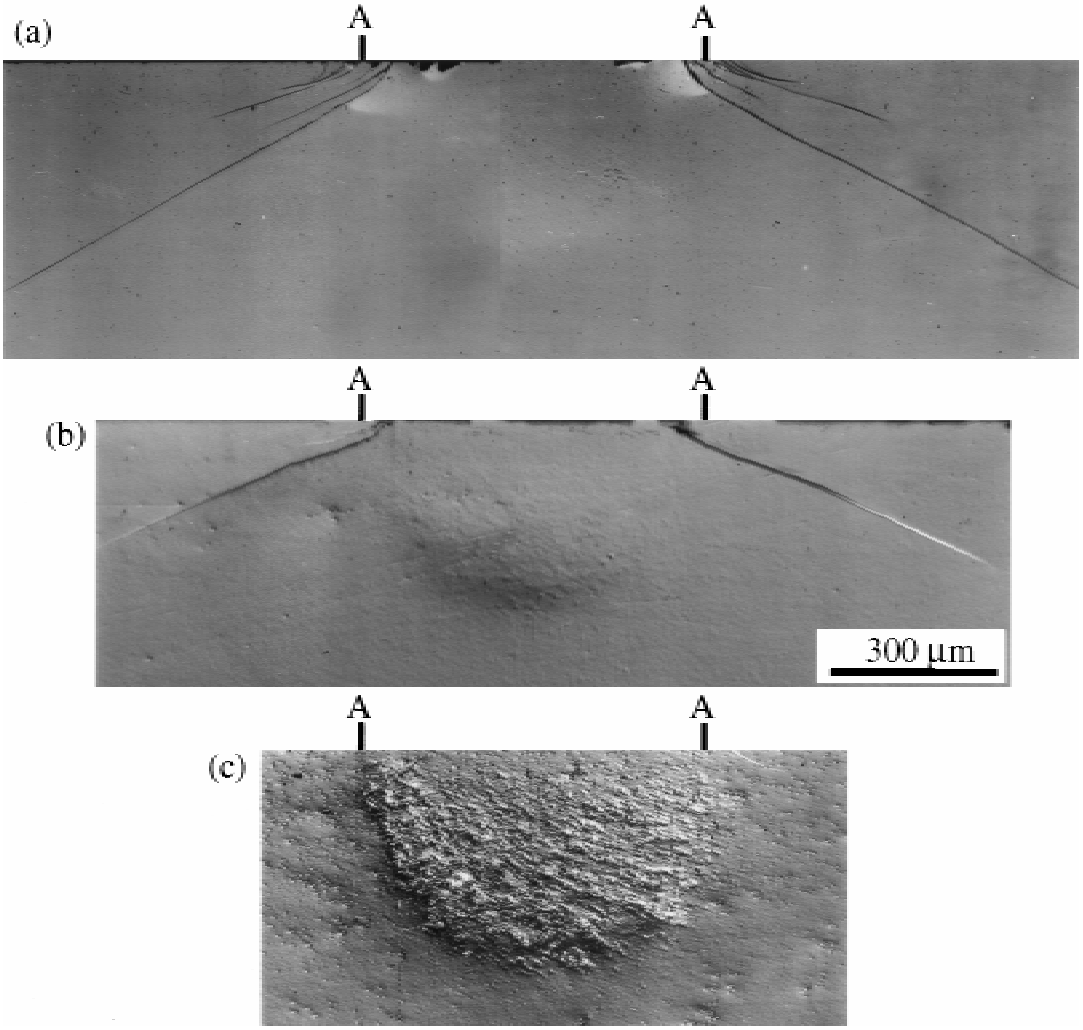

Fig. 6. Side views of Hertzian contact damage in **AC** Si_3N_4, fired at (a) 1650°, (b) 1700°, and (c) 1800°C. Indentations made using WC sphere radius $r = 1.98$ mm at load $P = 4000$ N. AA denotes contact diameter. Nomarski optical micrographs of bonded-interface specimens.

(2) Contact Damage

Figures 6–8 illustrate bonded-interface section views of contact damage formed at a relatively high load $P = 4000$ N, for the Si_3N_4 materials fired at 1650°, 1700°, and 1800°C:

(i) **AC** Si_3N_4, Fig. 6. (a) 1650°C—a classical cone crack forms outside the contact, indicative of a highly brittle material, and signs of minor quasi-plasticity damage are just visible beneath the contact; (b) 1700°C—the cone crack persists, but is smaller, and the quasi-plastic zone, although still comparatively minor, is more apparent; (c) 1800°C—only a barely visible shallow surface ring crack persists (more evident in surface views, not shown), but the quasi-plasticity zone is now well developed.[27]

(ii) **AF** Si_3N_4, Fig. 7. (a) 1650°C—a much shortened cone crack, and already a substantial quasi-plasticity zone, are apparent; (b) 1700°C—the damage zone is well developed, and only the vestigial trace of a surface ring crack remains; (c) 1800°C—the shallow ring crack is no longer visible in the section view (although, again, is evident in surface views), and the quasi-plasticity is now totally dominant. The ''brittle–ductile'' transition evident in this **AF** sequence is therefore similar to that in **AC**, but occurs much more rapidly.

(iii) **B** Si_3N_4, Fig. 8. (a) 1650°C—*both* cone cracking and quasi-plasticity zones are already well developed; (b) 1700°C—the cone cracking is reduced, and the quasi-plasticity further enhanced; (c) 1800°C—only shallow ring crack traces remain, and the plastic zone is dominant. The quasi-plasticity is more developed than in either **AC** or **AF**, and the cone cracking as strongly developed as in **AC**, foreshadowing a highly damage-susceptible material.

SEM observations confirmed previous observations of the microstructural nature of the damage processes: the cone and ring cracks in Figs. 6–8 were predominantly (>75%) intergranular;[27] and the quasi-plasticity zone consisted of individual shear faults at the grain boundaries, with some indication of some shear faulting within some of the elongate β grains.[20]

Figure 9 plots critical loads for yield, P_Y, and cracking, P_C, as a function of hot-pressing temperature. (Note that these P_Y and P_C data all lie below the value $P = 4000$ N used to produce the damage patterns in Figs. 6–8.) In Fig. 9(a), P_Y decreases steadily with firing temperature for **AC** and **AF** Si_3N_4, ultimately to the temperature-insensitive low value for **B** Si_3N_4. These temperature dependencies are broadly similar to those for the hardness (Fig. 4(b)), consistent with the well-documented interrelationship between yield stress and hardness.[30,31] This in turn implies a fundamental correlation between yield properties and β/α phase ratio (Fig. 5(b)). In Fig. 9(b), P_C increases only slightly with firing temperature (recall that the cracks contract from well-developed cones to very shallow surface rings at the higher temperatures). Values of P_C are highest for **AF**, lowest for **B**. These trends in the P_C data correlate with density of elongate β grains (Fig. 3(b) and (c)), consistent with the dominance of a microstructural geometry factor in the cone crack initiation.[27]

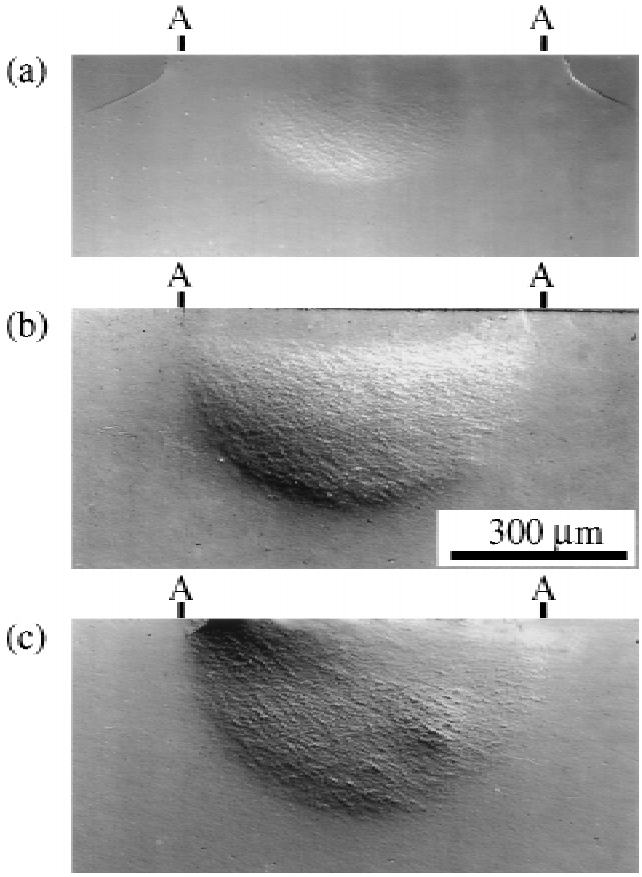

Fig. 7. Side views of Hertzian contact damage in **AF** Si_3N_4, fired at (a) 1650°, (b) 1700°, and (c) 1800°C. Indentations made using WC sphere radius $r = 1.98$ mm at load $P = 4000$ N. AA denotes contact diameter. Nomarski optical micrographs of bonded-interface specimens.

Figure 10 shows characteristic tensile-surface fracture patterns for **AF**, **AC**, and **B** Si_3N_4 bend-test specimens fired at 1700°C and damaged at contact load $P = 4000$ N:[28,34] in **AC** and **B**, fracture traces outside the ring-crack peripheries, corresponding to failures from subsurface cone-crack fronts (Figs. 10(a) and (c)); in **AF**, fracture traces orthogonal to the surface ring cracks, corresponding to failures from subsurface quasi-plastic zones (Fig. 10(b)) (in this case, the accompanying shallow ring cracks play no role). Figure 11 plots strength degradation data as a function of contact load P for the same materials. In each material the strengths remain undiminished at subcritical loads, indicating failures from natural flaws. Beyond critical loads, P_C for **AC** and **B**, $P_D \approx 2P_Y$ for **AF**[34] (see Fig. 9 at 1700°C) the strengths fall off slowly—solid curves in this region are data fits from fracture mechanics models (Appendix).

IV. Discussion

In the present study we have investigated the role of starting powder on Si_3N_4 microstructures (Figs. 1–5), and the relationship of these microstructures to damage accumulation in contacts with spheres (Figs. 6–10). We have shown that by controlling the starting powders and firing temperatures we can produce microstructures with different ratios of β to α phase (Fig. 2), and different grain sizes, shapes, and volume fractions of each phase (Fig. 3). These crystallographic and geometrical microstructural elements determine the competition between fracture (ring cracking) and deformation (diffuse quasi-plasticity) in concentrated stress fields. Specifically, for coarser, predominantly α-phase starting powder (**AC**), we produce steadily coarsening structures that retain their α-phase identity up to about 1700°C, with significant transformation to β phase only above this temperature. This material tends to be highly susceptible to cone cracking, with major quasi-plasticity only in specimens fired above 1700°C (Fig. 6). For finer α-phase powder (**AF**), the structures again coarsen, but much more rapidly with respect to temperature, and with larger volume fractions of elongate β grains. This material shows suppressed cracking and enhanced quasi-plasticity over the entire temperature range (Fig. 7). For the β-phase starting powder (**B**), the structures once more coarsen with temperature, although relatively slowly, and with retention of the β-phase identity throughout. Thus this material is highly susceptible to both fracture and deformation (Fig. 8).

It is of interest to identify more closely those elements of the Si_3N_4 microstructure that govern the deformation and fracture modes. Note that subsurface quasi-plasticity zones are equally well developed in all three materials at 1800°C in Figs. 6–8. (Recall that the hardnesses in Fig. 4(b) and critical loads P_Y in Fig. 9(a) each attain near-identical low values at this temperature.) The microstructural feature most closely common to the three materials at 1800°C is the near-saturation β content in Fig. 2. By contrast, there is no such commonality of grain size, shape, or density at 1800°C in Fig. 3. At 1650°C, the incidence of quasi-plasticity is barely lessened in the **B** material, but is substantially reduced in **AF** and even more in **AC**, consistent with reduced content of the relatively soft β phase in Fig. 2. For the fracture mode, we note that cone cracks are equally well developed in two of the materials at 1650°C, **B** and **AC**, and relatively suppressed in **AF**, in Figs. 6–8. (Also, the critical loads P_C in Fig. 9(b) are highest for **AF** at this temperature.) In this case there is no correlation between material order and β content in Fig. 2. On the other hand, **AF** has by far the most elongate β-grain shape in Fig. 3(b) and density in Fig. 3(c), if not the largest mean grain size in Fig. 3(a). At higher temperatures, cone cracking diminishes in all three materials, most abruptly between 1700° and 1800°C, where the density of β grains in Fig. 3(c) increases. We conclude that it is β content which constitutes the primary controlling factor in the quasi-plasticity mode, and β grain geometry in the fracture mode.

An important consideration in bearing and other stress-concentrating applications is retention of strength after the introduction of contact-related damage. The plots in Fig. 11 for the Si_3N_4 materials fired at 1700°C indicate that it is the **AF** structure that is most immune to strength degradation. That is because only shallow ring cracks form in this structure at and above 1700°C (Figs. 7(b) and 9(b)). In this context, the relative proliferation of large elongate β grains in the **AF**(1700) material (Fig. 1) is a key feature. It has been argued in an earlier study[27] that suppression of full cone fracture initiation in coarse, heterogeneous polycrystalline ceramics with intergranular fracture is attributable, at least in part, to intergranular deflection of the downward propagating ring cracks away from the trajectories of maximum tensile stresses in the contact field by such long grains. As we have intimated, the damage in **AF**(1700) (Fig. 7(b)) is instead distributed as highly stabilized, grain-localized shear faults within a dominant quasi-plasticity zone. Failure then occurs from one such fault within this zone, at a contact load P sufficiently in excess of P_Y to grow this fault to a dominant size (Appendix).[28,34] Ultimately, at excessive loads, or at a sufficiently large number of repeated contacts, microcrack coalescence may occur within the quasi-plastic zone, with reduction in strength to a level approximately equal to that for failure from cone cracks.[34] Nevertheless, for the single-cycle load range considered here, **AF** produced from the finer α-phase powder appears to be the Si_3N_4 material of choice for superior strength properties.

Our conclusions concerning the central role of microstructure on contact damage and associated strength degradation also have strong implications concerning mechanical properties like toughness and wear and fatigue resistance. Correlations between quasi-plastic contact damage and toughness have been

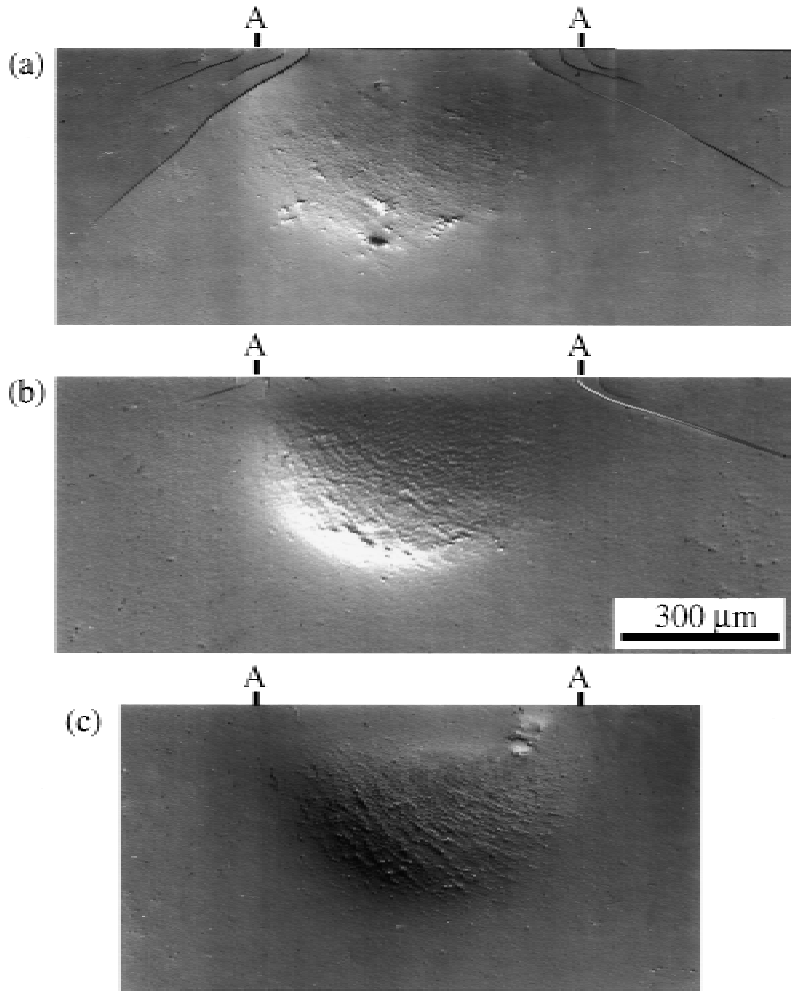

Fig. 8. Side views of Hertzian contact damage in **B** Si_3N_4, fired at (a) 1650°, (b) 1700°, and (c) 1800°C. Indentations made using WC sphere radius $r = 1.98$ mm at load $P = 4000$ N. AA denotes contact diameter. Nomarski optical micrographs of bonded-interface specimens.

noted in an earlier study.[27] There it was shown that reductions in the size of any well-developed cone cracks from microstructural coarsening and elongation can be attributed to enhancement of the underlying *R*-curve (hence long-crack toughness), via increased grain bridging.[16] Other groups[7,10–13] have demonstrated this link between microstructural heterogeneity and *R*-curve behavior even more compellingly. The connection between contact damage and toughness is not superficial: it is the same microstructural features responsible for steep *R*-curves (large and elongate grains, weak grain or interphase boundaries) that promote quasi-plasticity in the contact damage response, via weakness on the microscale.[29] The combination of suppressed cone cracking and limited quasi-plasticity evident for **AF** Si_3N_4 in Fig. 7 indicates that the microstructures sintered from the finer α-phase powder, because of their relatively pronounced microstructural heterogeneity, are the best suited of our materials for high toughness applications. At the same time, as noted for **B** Si_3N_4 in Fig. 8, it is possible to fabricate microstructures with both extensive quasi-plasticity *and* large cone cracks, so the existence of an extensive yield zone does not itself necessarily lead to high toughness—recall from Figs. 1 and 3(b) that the **B** material does not contain the elongate grains generally so effective in enhancing toughness.

From the standpoint of wear and fatigue, it is avoidance of quasi-plasticity (and only to a lesser extent ring cracking) that is important, because distributed microfailure damage can lead to easy removal of material on the microscale.[21,35–37] This suggests that the high modulus and hardness **AC** Si_3N_4 developed from coarser α-phase powder (Fig. 4) may be best suited for maximum wear and fatigue resistance.

Finally, we would emphasize that we have considered only two processing variables, starting powder and firing temperature. There are other important variables, most notably type and amount of additive oxides, that can have profound influences on the microstructural complexion of Si_3N_4 ceramics, especially on the composition of the oxynitride glassy phase.[10,11] More detailed and systematic investigations of chemical and geometrical aspects of the processing and microstructural characterization, in the special context of tailoring damage properties for specific applications, constitute a ripe area for further study.

APPENDIX

Fracture Mechanics Models for Failure from Indentation Cone Crack and Quasi-Plastic Damage Sites in Strength Tests

In this appendix we apply previously described fracture mechanics models for failure from cone cracks and quasi-plasticity zones[28,34] to fit the strength data in the region where breaks occur from indentation sites in Fig. 10.

(1) Failure from Cone Crack Sites

For the **AC** and **B** Si_3N_4 materials, failure occurs from cone cracks (Fig. 12). This kind of failure is governed by the following three simultaneous relations:[34]

(i) A geometrical relation connecting the dimension c of the actual ring crack to the dimension C of a ''virtual'' cone with its tip located above the contact surface,

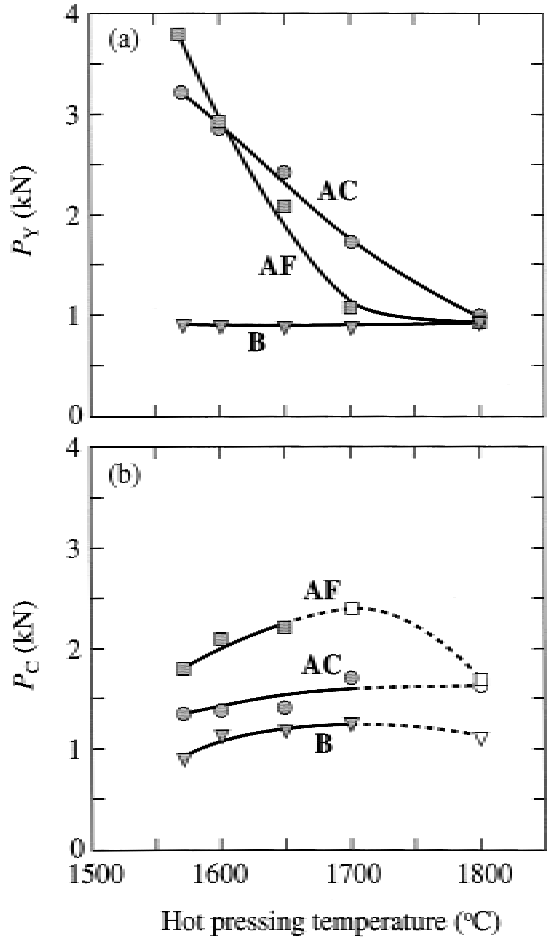

Fig. 9. Critical loads for indentation-induced damage as function of hot-pressing temperature, in **AC**, **AF**, and **B** Si_3N_4 materials: (a) P_Y for quasi-plastic damage; (b) P_C for ring cracking. Indentations made using WC sphere radius $r = 1.98$ mm. In (b), open symbols and solid curves denote full cone cracks, closed symbols and dashed curves denote very shallow surface ring cracks only.

$$C = c + R_0/\cos\alpha_0 \tag{A-1}$$

with R_0 the surface ring radius and α_0 the angle between cone crack and specimen surface (Fig. 12).

(ii) For materials governed by a single-valued toughness $K_{IC} = T_0$, an equilibrium stress-intensity factor relation for pennylike cracks,[38]

$$K = \chi P/C^{3/2} = T_0 \tag{A-2}$$

with χ a crack geometry coefficient. The parameter χ is calibrated from measurements of equilibrium cone crack lengths at given loads (e.g., Figs. 6 and 8), using $C = (\chi P/T_0)^{2/3}$.

(iii) The Griffith strength relation

$$\sigma_F = T_0/\Psi c^{1/2} \tag{A-3}$$

with Ψ a geometry coefficient determined from consideration of the cone crack geometry.[39]

The following parameters in Eqs. (A-1) to (A-3) are predetermined for **AC** and **B** Si_3N_4 (1700°C) as follows:

(i) In Eq. (A-1), cone angle $\alpha_0 = 19°$, and surface inner ring crack radius $R_0 = 238$ μm (**AC**) and 226 μm (**B**), from section micrographs (e.g., Figs. 6 and 8).

(ii) Coefficients in Eqs. (A-2) and (A-3), $\chi = 0.0154$ and $\Psi = 0.71$, from previous calibration on Si_3N_4 materials with similar cone crack geometry.[27,28]

(iii) In Eq. (A-3), toughness $K_{IC} = T_0 = 4.2$ MPa·m$^{1/2}$ (**AC**) and 3.0 MPa·m$^{1/2}$ (**B**), from independent measurements of radial cracks at Vickers indentations.[40]

The resulting calculated functions $\sigma_F(P)$ are included as the solid curves for **AC** Si_3N_4 and **B** Si_3N_4 in Fig. 11.

(2) Failure from Quasi-Plasticity Sites

For the **AF** Si_3N_4 material, failure occurs from ''wing'' cracks[41–43] associated with individual shear faults within the quasi-plasticity zones (Fig. 12).[34] This type of failure is governed by the strength relation[34]

$$\sigma_F = \sigma_0[(P_D^{1/3} - P_Y^{1/3})/(P^{1/3} - P_Y^{1/3})]^{1/3} \quad (P > P_D > P_Y) \tag{A-4}$$

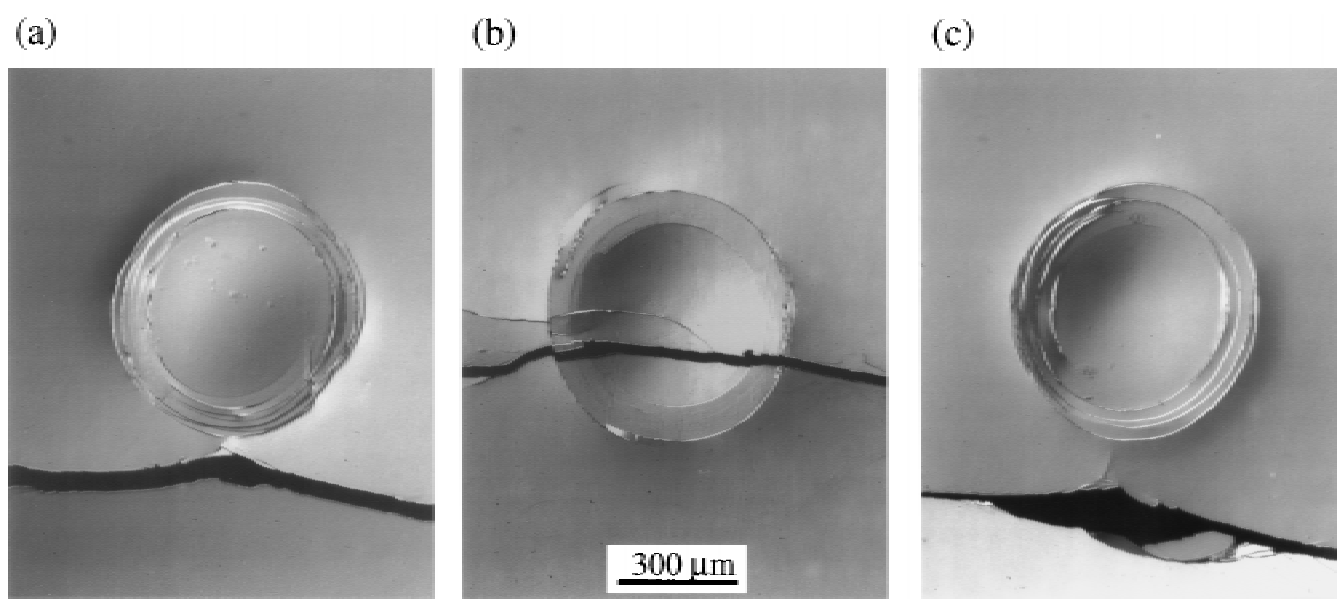

Fig. 10. Micrographs showing failure of (a) **AC**, (b) **AF**, and (c) **B** Si_3N_4 materials fired at 1700°C, from strength specimens containing indentations made with WC sphere, $r = 1.98$ mm, $P = 4000$ N. Nomarski illumination, surface gold coated. Tensile direction vertical in plane of diagram.

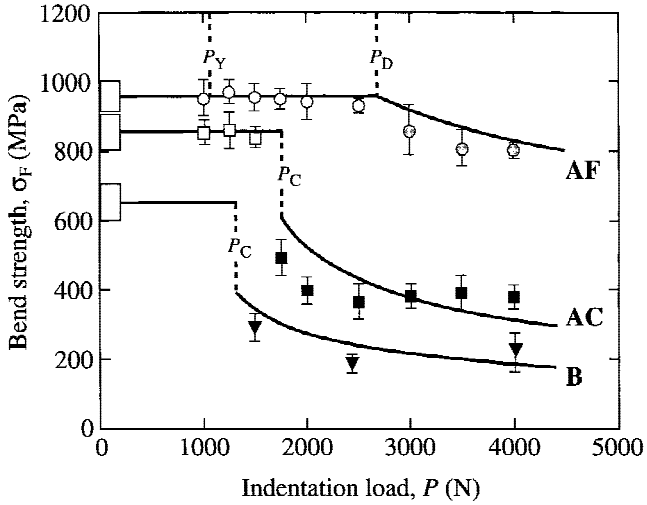

Fig. 11. Strength degradation for **AC**, **AF**, and **B** Si_3N_4 materials fired at 1700°C, for contacts with WC sphere, $r = 1.98$ mm. Open symbols indicate failures away from indentation sites, gray symbols failures from quasi-plastic zones, black symbols failures from ring cracks. Points with error bars represent means and standard deviations of a minimum of five specimens; points without error bars are individual breaks. Boxes at left axis denote natural strengths (unindented specimens). Vertical dashed lines indicate critical loads for strength-degrading damage (see Fig. 9).

where P_Y is the critical load for yield (Fig. 9(a), 1700°C), σ_0 is the natural strength (no indentation damage), and $P = P_D$ at $\sigma_F = \sigma_0$ is the load at which breaks first occur from the quasi-plasticity zone.

The solid curve for **AF** Si_3N_4 in Fig. 11 is obtained by inserting $\sigma_0 = 960$ MPa, $P_Y = 1100$ N, and $P_D = 2700$ N from a direct fit to the data.

Acknowledgments: We wish to thank H. H. K. Xu and I. M. Peterson for discussions.

References

[1]F. F. Lange, ''Relation Between Strength, Fracture Energy, and Microstructure of Hot-Pressed Si_3N_4,'' *J. Am. Ceram. Soc.*, **59** [10] 518–22 (1973).

[2]F. F. Lange, ''Fracture Toughness of Si_3N_4 as a Function of the Initial α-Phase Content,'' *J. Am. Ceram. Soc.*, **62** [7–8] 428–30 (1979).

[3]G. Himsolt, H. Knoch, H. Huebner, and F. W. Kleinlein, ''Mechanical Properties of Hot-Pressed Silicon Nitride with Different Grain Structures,'' *J. Am. Ceram. Soc.*, **62** [1–2] 29–32 (1979).

[4]G. Wötting and G. Ziegler, ''Influence of Powder Properties and Processing Conditions on Microstructure and Mechanical Properties of Sintered Si_3N_4,'' *Ceram. Int.*, **10** [1] 18–22 (1984).

[5]C.-W. Li and J. Yamanis, ''Super-Tough Silicon Nitride with *R*-Curve Behavior,'' *Ceram. Eng. Sci. Proc.*, **10** [7–8] 632–45 (1989).

[6]T. Kawashima, H. Okamoto, H. Yamamoto, and A. Kitamura, ''Grain Size Dependence of the Fracture Toughness of Silicon Nitrides Ceramics,'' *J. Ceram. Soc. Jpn.*, **99**, 1–4 (1991).

[7]C.-W. Li, D.-J. Lee, and S.-C. Lui, ''*R*-Curve Behavior and Strength of *In Situ* Reinforced Silicon Nitride with Different Microstructures,'' *J. Am. Ceram. Soc.*, **75** [7] 1777–85 (1992).

[8]N. Hirosaki and Y. Akimune, ''Effect of Grain Growth of β-Silicon Nitride on Strength, Weibull Modulus, and Fracture Toughness,'' *J. Am. Ceram. Soc.*, **76** [7] 1892–94 (1993).

[9]A. J. Pyzik and D. R. Beaman, ''Microstructure and Properties of Self-Reinforced Silicon Nitride,'' *J. Am. Ceram. Soc.*, **76** [11] 2737–44 (1993).

[10]P. F. Becher, S. L. Hwang, H. T. Lin, and T. N. Tiegs, ''Microstructural Contributions to the Fracture Resistance of Silicon Nitride Ceramics''; pp. 87–100 in *Tailoring of Mechanical Properties of Si_3N_4*. Edited by M. J. Hoffmann and G. Petzow. Kluwer Academic Publishers, Dordrecht, Netherlands, 1994.

[11]M. J. Hoffmann, ''Analysis of Microstructural Development and Mechanical Properties of Si_3N_4''; pp. 59–72 in *Tailoring of Mechanical Properties of Si_3N_4*. Edited by M. J. Hoffmann and G. Petzow. Kluwer Academic Publishers, Dordrecht, Netherlands, 1994.

[12]P. Sajgalik, J. Dusza, and M. J. Hoffmann, ''Relationship between Microstructure, Toughness Mechanisms, and Fracture Toughness of Reinforced Silicon Nitride Ceramics,'' *J. Am. Ceram. Soc.*, **78** [10] 2619–24 (1995).

[13]C.-W. Li, S.-C. Lui, and J. Goldacker, ''Relation Between Strength, Microstructure, and Grain-Bridging Characteristics in *In Situ* Reinforced Silicon Nitride,'' *J. Am. Ceram. Soc.*, **78** [2] 449–59 (1995).

[14]M. Mitomo, M. Tsutsumi, H. Tanaka, S. Uenosono, and F. Saito, ''Grain Growth During Gas-Pressure Sintering of β-Silicon Nitride,'' *J. Am. Ceram. Soc.*, **73** [8] 2441–45 (1990).

[15]M. Mitomo and S. Uenosono, ''Microstructural Development During Gas-Pressure Sintering of α-Silicon Nitride,'' *J. Am. Ceram. Soc.*, **75** [1] 103–108 (1992).

[16]P. L. Swanson, C. J. Fairbanks, B. R. Lawn, Y.-W. Mai, and B. J. Hockey, ''Crack-Interface Grain Bridging as a Fracture Resistance Mechanism in Ceramics: I, Experimental Study on Alumina,'' *J. Am. Ceram. Soc.*, **70** [4] 279–89 (1987).

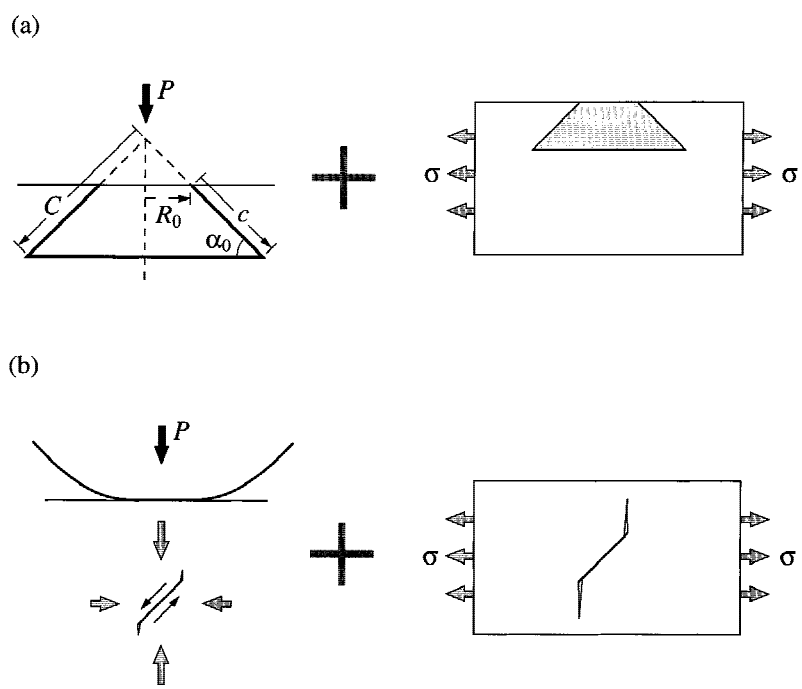

Fig. 12. Schematic showing critical flaws induced by contact with spherical indenter (left), and subsequent strength tests on indented specimens (right): (a) brittle response, failure from fully developed cone crack; (b) quasi-plastic response, failure from shear fault with wing crack within damage zone. After Refs. 28 and 34.

[17]S. J. Bennison and B. R. Lawn, ''Role of Interfacial Grain-Bridging Sliding Friction in the Crack-Resistance and Strength Properties of Nontransforming Ceramics,'' *Acta Metall.*, **37** [10] 2659–71 (1989).

[18]B. R. Lawn, *Fracture of Brittle Solids*; Ch. 7. Cambridge University Press, Cambridge, U.K., 1993.

[19]N. P. Padture, J. L. Runyan, S. J. Bennison, L. M. Braun, and B. R. Lawn, ''Model for Toughness-Curves in Two-Phase Ceramics: II, Microstructural Variables,'' *J. Am. Ceram. Soc.*, **76** [9] 2241–47 (1993).

[20]H. H. K. Xu, L. Wei, N. P. Padture, B. R. Lawn, and R. L. Yeckley, ''Effect of Microstructural Coarsening on Hertzian Contact Damage in Silicon Nitride,'' *J. Mater. Sci.*, **30**, 869–78 (1995).

[21]H. H. K. Xu, S. Jahanmir, and L. K. Ives, ''Material Removal and Damage Formation Mechanisms in Grinding Silicon Nitride,'' *J. Mater. Res.*, **11** [7] 1717–24 (1996).

[22]F. Guiberteau, N. P. Padture, H. Cai, and B. R. Lawn, ''Indentation Fatigue: A Simple Cyclic Hertzian Test for Measuring Damage Accumulation in Polycrystalline Ceramics,'' *Philos. Mag. A*, **68** [5] 1003–16 (1993).

[23]H. Cai, M. A. Stevens Kalceff, and B. R. Lawn, ''Deformation and Fracture of Mica-Containing Glass-Ceramics in Hertzian Contacts,'' *J. Mater. Res.*, **9** [3] 762–70 (1994).

[24]F. Guiberteau, N. P. Padture, and B. R. Lawn, ''Effect of Grain Size on Hertzian Contact in Alumina,'' *J. Am. Ceram. Soc.*, **77** [7] 1825–31 (1994).

[25]A. Pajares, F. Guiberteau, B. R. Lawn, and S. Lathabai, ''Hertzian Contact Damage in Magnesia-Partially-Stabilized Zirconia,'' *J. Am. Ceram. Soc.*, **78** [4] 1083–86 (1995).

[26]N. P. Padture and B. R. Lawn, ''Toughness Properties of a Silicon Carbide with an *In-Situ*-Induced Heterogeneous Grain Structure,'' *J. Am. Ceram. Soc.*, **77** [10] 2518–22 (1994).

[27]S. K. Lee, S. Wuttiphan, and B. R. Lawn, ''Role of Microstructure in Hertzian Contact Damage in Silicon Nitride: I, Mechanical Characterization,'' *J. Am. Ceram. Soc.*, **80** [9] 2367–81 (1997).

[28]S. K. Lee and B. R. Lawn, ''Role of Microstructure in Hertzian Contact Damage in Silicon Nitride: II, Strength Degradation,'' *J. Am. Ceram. Soc.*, **81** [4] 997–1003 (1998).

[29]B. R. Lawn, N. P. Padture, H. Cai, and F. Guiberteau, ''Making Ceramics 'Ductile','' *Science*, **263**, 1114–16 (1994).

[30]A. C. Fischer-Cripps and B. R. Lawn, ''Stress Analysis of Contact Deformation in Quasi-Plastic Ceramics,'' *J. Am. Ceram. Soc.*, **79** [10] 2609–18 (1996).

[31]D. Tabor, *Hardness of Metals.* Clarendon, Oxford, U.K., 1951.

[32]H. Makino, N. Kamiya, and S. Wada, ''Grain Size Effects of Si_3N_4 on Damage Morphology Induced by Localized Contact Stress''; pp. 229–34 in *Proceedings of the 1st International Symposium on the Science of Engineering Ceramics.* Edited by S. Kimura and K. Niihara. Koda, Aichi-Prefecture, Japan, 1991.

[33]C. Greskovich and G. E. Gazza, ''Hardness of Dense α- and β-Si_3N_4 Ceramics,'' *J. Mater. Sci. Lett.*, **4**, 195–96 (1985).

[34]B. R. Lawn, S. K. Lee, I. M. Peterson, and S. Wuttiphan, ''A Model of Strength Degradation from Hertzian Contact Damage in Tough Ceramics,'' *J. Am. Ceram. Soc.*, **81** [6] 1509–20 (1998).

[35]N. P. Padture and B. R. Lawn, ''Contact Fatigue of a Silicon Carbide with a Heterogeneous Grain Structure,'' *J. Am. Ceram. Soc.*, **78** [6] 1431–38 (1995).

[36]N. P. Padture and B. R. Lawn, ''Fatigue in Ceramics with Interconnecting Weak Interfaces: A Study Using Cyclic Hertzian Contacts,'' *Acta Metall.*, **43** [4] 1609–17 (1995).

[37]H. H. K. Xu, S. Jahanmir, L. K. Ives, L. S. Job, and K. T. Ritchie, ''Short-Crack Toughness and Abrasive Machining of Silicon Nitride,'' *J. Am. Ceram. Soc.*, **79** [12] 3055–64 (1996).

[38]B. R. Lawn and T. R. Wilshaw, ''Indentation Fracture: Principles and Applications,'' *J. Mater. Sci.*, **10** [6] 1049–81 (1975).

[39]B. R. Lawn, S. M. Wiederhorn, and H. Johnson, ''Strength Degradation of Brittle Surfaces: Blunt Indenters,'' *J. Am. Ceram. Soc.*, **58** [9–10] 428–32 (1975).

[40]G. R. Anstis, P. Chantikul, D. B. Marshall, and B. R. Lawn, ''A Critical Evaluation of Indentation Techniques for Measuring Fracture Toughness: I, Direct Crack Measurements,'' *J. Am. Ceram. Soc.*, **64** [9] 533–38 (1981).

[41]H. Horii and S. Nemat-Nasser, ''Compression-Induced Microcrack Growth in Brittle Solids: Axial Splitting and Shear Failure,'' *J. Geophys. Res.*, **90** [B4] 3105–25 (1985).

[42]H. Horii and S. Nemat-Nasser, ''Brittle Failure in Compression: Splitting, Faulting and Brittle–Ductile Transition,'' *Philos. Trans. R. Soc. London*, **319** [1549] 337–74 (1986).

[43]M. F. Ashby and S. D. Hallam, ''The Failure of Brittle Solids Containing Small Cracks Under Compressive Stress States,'' *Acta Metall. Mater.*, **34** [3] 497–510 (1986). □